Inorganic Chemistry

Article

pubs.acs.org/IC

Coexistence of Monochalcogen and Dichalcogen Ions in $BiSe_2$ and BiS_2 Crystals Prepared at High Pressure

Ayako Yamamoto,*[,†] Daisuke Hashizume,[†] Mohammad Saeed Bahramy,[†,‡] and Yoshinori Tokura[†,‡]

[†]Center for Emergent Matter Science, RIKEN, Saitama 351-0198, Japan

[‡]Department of Applied Physics and Quantum-Phase Electronics Center, The University of Tokyo, Tokyo 113-8656, Japan

Supporting Information

ABSTRACT: A single crystal of bismuth diselenide, $BiSe_2$, containing both monochalcogen (Se^{2-}) and dichalcogen (Se_2^{2-}) ions, was prepared at a high pressure of 5.5 GPa. Its crystal structure, substitution chemistry, and physical properties were investigated. X-ray analysis showed that $BiSe_2$ is in a monoclinic system (space group $C2/m$) with the following lattice parameters: a = 16.740(3) Å, b = 4.1410(11) Å, c = 12.027(3) Å, and β = 127.658(13)°. A crystal structure of $BiSe_2$ can be viewed as a layered structure with stacks of neutral $BiSe_2$ blocks along the c-axis, or alternatively as a quasi-one-dimensional structure with double chains of $BiSe_5$ pyramids along the b-axis. Each Bi is coordinated with three Se^{2-} ions and two Se_2^{2-} ions, and the bond valence analysis indicated that Bi was trivalent. $BiSe_2$ and BiS_2 form a solid solution in the whole range while retaining the same structure, and the partial substitution of Sb for Bi is also achieved at 10%. All the compounds show a semiconducting property and diamagnetism that can be attributed to the closed-shell ion core. In spite of the compositional analogy with Bi_2Se_3, $BiSe_2$ is proven by the first-principles calculations not to be a topological insulator.

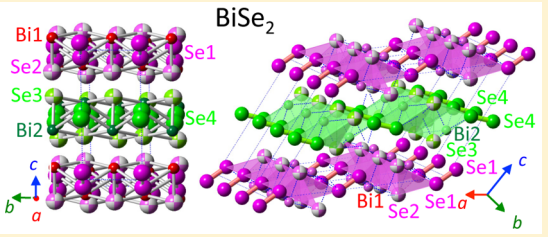

1. INTRODUCTION

Bismuth chalcogenides Bi_2X_3 (X = S, Se, and Te) have been among the most attractive compounds because of their unique physical and chemical properties. In particular, this is true for Bi_2Se_3 and Bi_2Te_3, which show high thermoelectric performance[1] as well as a robust surface metallic state as three-dimensional topological insulators.[2] Bismuth chalcogenides are also interesting in light of structural variations at high pressure; Bi_2Se_3 has four polymorphic phases below 10 GPa,[3] and Bi_2Te_3 has also several polymorphic phases,[4] one of which shows superconductivity with a T_c of 5 K at 13 GPa.[5]

In conventional bismuth chalcogenides Bi_2X_3, Bi and X are trivalent and divalent, respectively. Therefore, the ratio of chalcogen to Bi should be 3/2. The sole exception is the case of BiS_2 and $BiSe_2$, which were synthesized at a high pressure of 4.5 GPa by Silverman et al.[6,7] They reported the composition and peak positions of the X-ray powder diffraction (XRD) patterns of the products, but the crystal structure and physical properties have not been clarified. If BiS_2 and $BiSe_2$ are obtained as a single phase and the composition is stoichiometric, it is very interesting from a coordination chemistry viewpoint; a part of the bismuth or chalcogen should take a different valence in the solid. A possible case would be that a part of chalcogens form S_2^{2-} or Se_2^{2-} as seen in $IrSe_2$[8] or $RhSe_2$.[9] Alternatively, a mixed-valence state of bismuth as in $BaBiO_3$[10] may not be excluded. In any case, the structure and properties of the novel Bi dichalcogenides are worth exploring for their unconventional properties.

Recently, superconductivity in several bismuth oxysulfides, e.g., $LaO_{1-x}F_xBiS_2$, has been reported.[11] All these compounds have a layered structure composed of BiS_2 sheets, which play an essential role in the superconductivity.[12] To the best of our knowledge, however, there has been no known compound comprising only BiS_2 layers. If such a compound is realized, it may provide a clue to understanding the superconductivity of the BiS_2 layer. In this study, we have succeeded in obtaining single crystals of $BiSe_2$, BiS_2, and its solid solutions from the melt at 5.5 GPa. The crystal structure was determined using single-crystal XRD analysis. Thermal, transport, and magnetic properties were measured and analyzed with reference to the band structure, which was calculated using the obtained structural data. The coordination chemistry between bismuth and chalcogen is also discussed.

2. EXPERIMENTAL SECTION

Samples were prepared from Bi_2Se_3 (99.9%), Bi_2S_3 (99.99%), Se (99.999%), and S (99.99%) with a Bi:S/Se mole ratio of 1.0:2.2−3.0. Excess S/Se was needed to suppress residual products of Bi_2Se_3/Bi_2S_3. Solid solutions, $Bi(Se_{1-y}X_y)_2$ (X = S or Te) and $(Bi_{1-y}M_y)Se_2$ (M = Pb or Sb), were also synthesized using Te (99.9%), Pb (99.99%), and Sb (99.9%). Approximately 400 mg of a mixture of raw materials was pressed into a cylindrical shape (3.9 mm in diameter and 6.0 mm in height), placed in a BN container, and inserted into a carbon tube heater. It was pressurized at 3.0, 5.5, and 7.5 GPa using a cubic-anvil-type press (700 ton, TRY Eng. Co.) and heated at 650−1200 °C for 10−30 min. Single crystals were grown from the melt with a cooling rate of 5 °C/min from 1200 to 800 °C and subsequent quenching to

Received: February 14, 2015
Published: April 9, 2015

DOI: 10.1021/acs.inorgchem.5b00349
Inorg. Chem. 2015, 54, 4114−4119

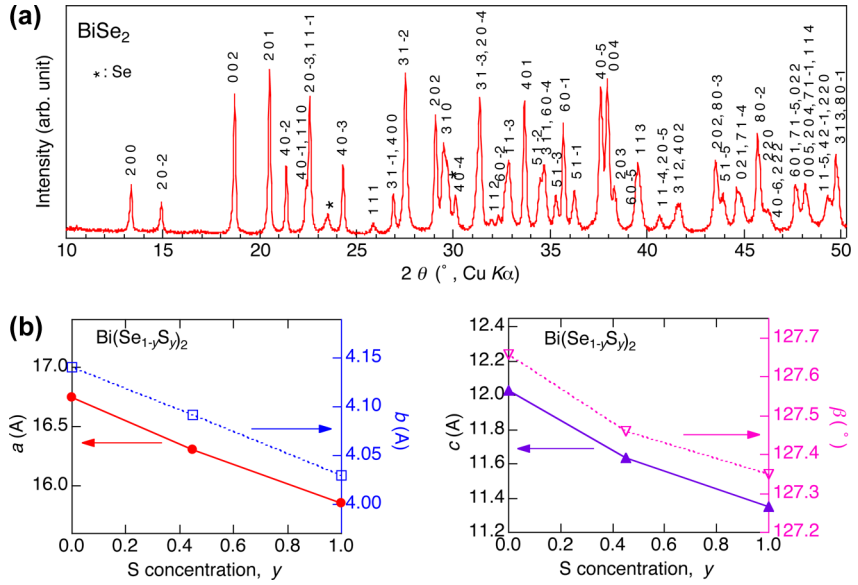

Figure 1. (a) Powder X-ray diffraction pattern of $BiSe_2$. The peaks are compatibly indexed with structural refinement of single-crystal X-ray diffraction data. (b) Compositional dependence of the lattice parameters of $Bi(Se_{1-y}S_y)_2$ (y = 0, 0.5, or 1.0).

room temperature. Residual Se and S were removed by washing the product with carbon disulfide.

X-ray powder diffraction patterns of the powderized crystal were measured with Cu Kα radiation using a diffractometer (RigakuRINT). The chemical composition was determined using energy dispersive X-ray analysis (Bruker AXS, XFlash detector 5030) of a scanning electron microscope (JEOL, JSM-6701F). The crystal structures were determined by single-crystal XRD analysis using diffraction data measured with a four-circle diffractometer equipped with a Saturn70 CCD detector (Rigaku, AFC-8 with a Mo rotating anode).

The thermal stability of the products was studied using a thermobalance (Rigaku, Thermo Plus evo); 10 mg of powered samples in an aluminum cell was heated (5 °C/min) from 20 to 800 °C with flowing high-purity Ar. The electrical resistivity was measured with a picoammeter voltage source (Keithley 6487) (0.1−10 V applied from 300 to 50 K, V//b); the resistivity was too high to measure with a conventional measurement system (Quantum Design, PPMS). The contact between the sample and gold wire was taken with silver paste (Dupont 4929). The dc susceptibility was measured with $\mu_0 H$ = 1 T using a magnetic property measurement system (Quantum Design, MPMS).

Electronic structure calculations were performed within the context of density functional theory using the Perdew−Burke−Ernzerhof exchange-correlation functional, as implemented in WIEN2K.[13] Relativistic effects, including spin−orbit coupling, were fully included. The muffin-tin radius of each atom (R_{MT}) was chosen such that its product with the maximal modulus of reciprocal vectors K_{max} becomes $R_{MT}K_{max}$ = 7.0. The lattice parameters and atomic positions of $BiSe_2$ were taken from the crystal structure analyses presented here, whereas for Bi_2Se_3, we used the structural data reported in ref 14. For $BiSe_2$ (Bi_2Se_3), the corresponding Brillouin zone was sampled by a 4 × 14 × 6 (10 × 10 × 3) k-mesh.

3. RESULTS AND DISCUSSION

3.1. Synthesis and Characterization. To obtain a single phase of $BiSe_2$, we have examined various synthetic conditions of pressures, temperatures, and starting compositions. In the synthesis at 3.0 GPa, the starting materials did not react at all even above 900 °C while at 5.5 GPa showed a different phase, i.e., that we have investigated in this study. Polycrystalline and single-crystalline samples were obtained at approximately 700 and 1100 °C, respectively. In the synthesis at 7.5 GPa, an unknown phase appeared; it turned out to be a polymorph of $BiSe_2$ that will be reported elsewhere.

We have also examined the effect of the nominal composition on the phase purity of $BiSe_2$. Samples were synthesized with 10 and 50% excesses of Se and analyzed using scanning electron microscopy (SEM) equipped with energy dispersive X-ray analyzer (EDX). The samples with a 10% excess included a considerable amount of Bi_2Se_3, while those with a 50% excess do not but had extra Se. Because a mixed-in Se simple substance can be easily removed with carbon disulfide, we adopted the starting composition with a 50% excess of Se. The powder XRD pattern of $BiSe_2$ is shown in Figure 1a.

The obtained single crystals of $BiSe_2$ and substitutions are of a silver-black color and columnar shape, as shown in Figure 2a. The typical size of the crystal was 200 μm long and 20 μm wide. The flat terraces observed by SEM indicate a cleavage property, as shown in Figure 2b. The compositions of the crystals are quite stoichiometric, and the values are summarized in Table 1.

Using the same synthetic conditions, solid solutions of $Bi(Se_{1-y}S_y)_2$ (y = 0.5 or 1.0), $Bi(Se_{1-y}Te_y)_2$ (y = 0.1, 0.33, or 1.0), and $(Bi_{1-y}Sb_y)Se_2$ (y = 0.1), and $(Bi_{1-y}Pb_y)Se_2$ (y = 0.1) have been prepared to investigate effects of chalcogen anion size and carrier doping on the physical properties. $Bi(Se_{1-y}S_y)_2$ was observed to form a solid solution over the whole range while retaining its structure. The analyzed compositions and refined lattice parameters of the sulfur-substituted samples are listed in Table 1 and plotted in Figure 1(panel b). For the tellurium-doped sample $Bi(Se_{1-y}Te_y)_2$, the composition analysis suggests that the ratio of Bi to (Se+Te) is close to 1:2, at least for y = 0.1. However, the XRD pattern indicated that the structure of the product is not identical to that of $BiSe_2$. The number of diffraction lines is small, and the intensity is high, suggesting a higher symmetry in the structure of $Bi(Se_{0.9}Te_{0.1})_2$. Next, we tested the substitution of the Bi site using isovalent and smaller-sized Sb^{3+} and heterovalent and comparably sized Pb^{2+}. Sb can replace at least 10% of the Bi site. Pb could not substitute for Bi under this condition, in contrast to the fact

DOI: 10.1021/acs.inorgchem.5b00349
Inorg. Chem. 2015, 54, 4114−4119

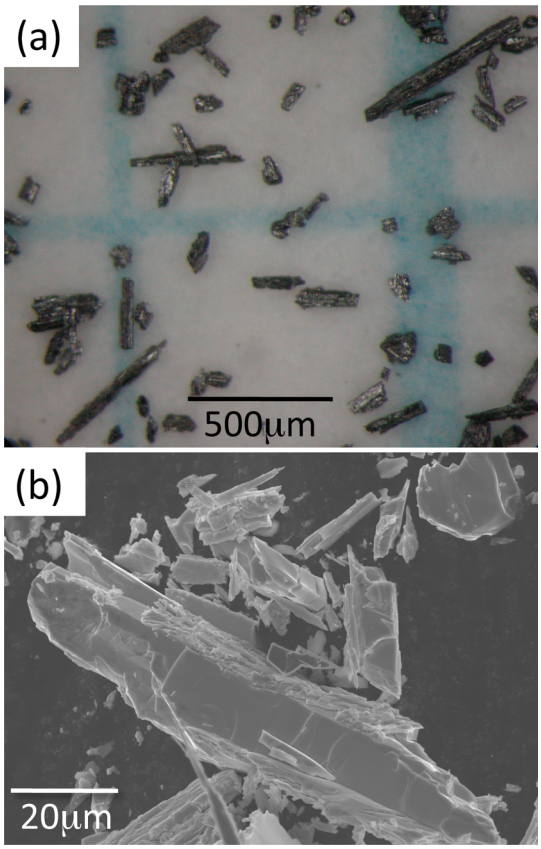

Figure 2. (a) Optical photomicrograph of $BiSe_2$ crystals. (b) SEM image of BiSSe crystals.

that Bi substitution in the form of $(Pb_{1-x}Bi_x)Se_2$ is possible up to $x = 0.2$ at high pressure.[15] The lattice parameters of $(Bi_{0.9}Sb_{0.1})Se_2$ are slightly smaller than those of the pristine form, as listed in Table 1. The chemical and physical properties of the substituted samples are also discussed below.

3.2. Crystal Structure and Bonding Characters. The single-crystal X-ray analysis of $BiSe_2$ indicates a monoclinic cell (No. 12, $C2/m$) with the following lattice parameters: a = 16.740(3) Å, b = 4.1410(11) Å, c = 12.027(3) Å, β = 127.658(13)°. Refined atomic positions are listed in Table 2 and further details in the Supporting Information. The structure is complicated beyond expectation from the simple composition, in contrast to the structure of Bi_2Se_3 with high symmetry. The density of $BiSe_2$ is 7.385 g/cm^3, and this corresponds to an 18% reduction from the averaged density of the starting materials (Bi_2Se_3 and Se, 6.051 g/cm^3). As shown in Table 2, Bi and Se have two distinct sites and four distinct sites, respectively, but Bi1 and Bi2, Se1 and Se4, and Se2 and Se3 are basically comparable. The crystal structure of $BiSe_2$ can be considered as a layered structure with stacks of neutral $BiSe_2$ blocks perpendicular to the c-axis (see Figure 3a). The bonding between the layers appears to be weak, and the crystal can be easily cleaved at this plane as seen in Figure 2b. The crystal structure is also viewed as the quasi-one-dimensional one with double chains of a $BiSe_5$ pyramid along the b-axis (Figure 3b), which may work as a carrier conduction path.

The characteristic feature of this structure is that two types of ions, diselenium and monoselenium ions, coexist in one compound as shown in Figure 3d. Such coexistence is observed in orthorhombic $IrSe_2$[8] and $RhSe_2$.[9] The local coordination of Bi and Se is depicted in Figure 3c together with the bond distances. Se1 forms a Se dimer with a short distance of 2.375 Å, which is shorter than that of $IrSe_2$ (Se−Se, 2.555 Å)[8] but very close to that of the Se dimer in $PbSe_2$[15] (Se−Se, 2.325 Å) and $PdSe_2$[16] (Se−Se, 2.36 Å). Because these Se dimers are Se_2^{2-}, the dimer in $BiSe_2$ is also anticipated to be divalent. Se1 is coordinated with not only Se but also Bi with a standard distance of 3.005 Å (×2) while Se2 with three Bi1 atoms with distances of 2.734 Å (×1) and 2.922 Å (×2). When viewed from Bi1, Bi is coordinated with two Se1 and three Se2 atoms. This five coordination is opposite to the tendency that the high-pressure phase prefers a coordination number (CN) higher than that of the ambient-pressure phase (cf. the CN of Bi in Bi_2Se_3 is six). To determine the valence of Bi, a bond-valence sum[17] was calculated using the Bi−Se distances. The sum is +2.97 for Bi1 and +2.95 for Bi2, which are comparable to the value of +2.81 for Bi in Bi_2Se_3,[18] provided that the valence of Bi is trivalent.

Thus, the charge neutrality of $BiSe_2$ is satisfied with formal valences of Bi^{3+}, $0.5Se_2^{2-}$, and Se^{2-}. This confirms that each $BiSe_2$ layer perpendicular to the c-axis is neutral in charge and that bonding between layers is weak. However, the actual interlayer distance (1.7 Å) is much shorter than that in $MoSe_2$ (3.2 Å),[19] which is typical of a van der Waals bond. The lone

Table 1. Compositions, Lattice Parameters, and Properties of $BiSe_2$ and Its Substitutions Prepared at 5.5 GPa

composition	analyzed composition	a (Å)	b (Å)	c (Å)	β (deg)	V (Å^3)
$BiSe_2$[a]	1.00(2):2.00(2) Bi:Se	16.740(3)	4.1410(11)	12.027(3)	127.658(13)	660.0(3)
BiSSe[a]	1.00(2):0.88(2):1.12(3) Bi:S:Se	16.3670(12)	4.1040(4)	11.6772(13)	127.401(4)	623.10(11)
BiS_2[a]	1.02(1):1.98(1) Bi:S	15.7879(14)	4.0261(7)	11.3330(19)	127.562(8)	571.03(15)
$(Bi_{0.9}Sb_{0.1})Se_2$[b]	0.89(6):0.10(1):2.01(6) Bi:Sb:Se	16.64(6)	4.136(9)	11.93(4)	128.4(2)	643.5(4)
$Bi(Se_{0.9}Te_{0.1})_2$[c]	1.00(2):1.88(2):0.12(3) Bi:Se:Te	–	–	–	–	–

composition	decomposition temp (°C)[d]	susceptibility (emu/mol)	band gap (=$2E_a$,[f] eV)
$BiSe_2$[a]	285	-8.8×10^{-5} (calcd -9.5×10^{-5})[e]	0.61
BiSSe[a]	239	-7.1×10^{-5} (calcd -8.0×10^{-5})	0.28
BiS_2[a]	256	-6.3×10^{-5} (calcd -6.5×10^{-5})	0.66
$(Bi_{0.9}Sb_{0.1})Se_2$[b]	–	-7.5×10^{-5}	0.69
$Bi(Se_{0.9}Te_{0.1})_2$[c]	–	–	–

[a]Lattice parameters were determined by single-XRD analyses. [b]Lattice parameters were determined by powder XRD analysis. [c]The crystal structure is different from that of $BiSe_2$, which has not been determined. [d]The decomposition temperatures were determined with the intersection point between the baseline and the tangential lines along the distinct weight loss. [e]Calculation based on the data from ref 21. [f]The band gap, E_g, corresponds to twice the activation energy, $2E_a$.

DOI: 10.1021/acs.inorgchem.5b00349
Inorg. Chem. 2015, 54, 4114−4119

Table 2. Atomic Positions of $BiSe_2$, BiSSe, and BiS_2 Refined by Single-X-ray Diffraction Analysis

(a) $BiSe_2$, R = 9.89%

atom	site	g^a	x	y	z	U_{iso} (Å^2)^b
Bi1	4*i*	1	0.69853(13)	0	0.09377(18)	0.0494(7)
Bi2	4*i*	1	0.38976(12)	0	0.60685(18)	0.0519(8)
Se1	4*i*	1	0.5348(3)	1/2	0.9386(5)	0.0495(11)
Se2	4*i*	1	0.6536(3)	0	0.8337(4)	0.0460(10)
Se3	4*i*	1	0.2112(3)	0	0.3427(4)	0.0454(11)
Se4	4*i*	1	0.4146(3)	1/2	0.4550(5)	0.0489(11)

(b) BiSeS ($BiSe_{1.12}S_{0.88}$), R = 5.70%

atom	site	g^c	x	y	z	U_{iso} (Å^2)
Bi1	4*i*	1	0.70141(5)	0	0.09850(7)	0.0492(2)
Bi2	4*i*	1	0.38951(5)	0	0.60895(8)	0.0511(2)
Se1/S1	4*i*	0.824(14)/0.176(14)	0.53498(15)	1/2	0.9385(2)	0.0492(7)
Se2/S2	4*i*	0.479(14)/0.521(14)	0.65381(18)	0	0.8351(3)	0.0432(8)
Se3/S3	4*i*	0.328(14)/0.672(14)	0.2122(2)	0	0.3452(3)	0.0440(9)
Se4/S4	4*i*	0.545(13)/0.455(13)	0.41744(18)	1/2	0.4584(3)	0.0448(8)

(c) BiS_2, R = 4.97%

atom	site	g	x	y	z	U_{iso} (Å^2)
Bi1	4*i*	1	0.70169(4)	0	0.10213(5)	0.0471(2)
Bi2	4*i*	1	0.39353(4)	0	0.61364(6)	0.0425(6)
Se1	4*i*	1	0.5341(2)	1/2	0.9452(4)	0.0475(2)
Se2	4*i*	1	0.6558(2)	0	0.8391(3)	0.0473(6)
Se3	4*i*	1	0.2131(2)	0	0.3472(3)	0.0435(6)
Se4	4*i*	1	0.4226(2)	1/2	0.4635(4)	0.0452(6)

^{a}Occupancy factor. ^{b}Isotropic atomic displacement parameter. ^{c}g was fixed as g(Se) + g(S) = 1.

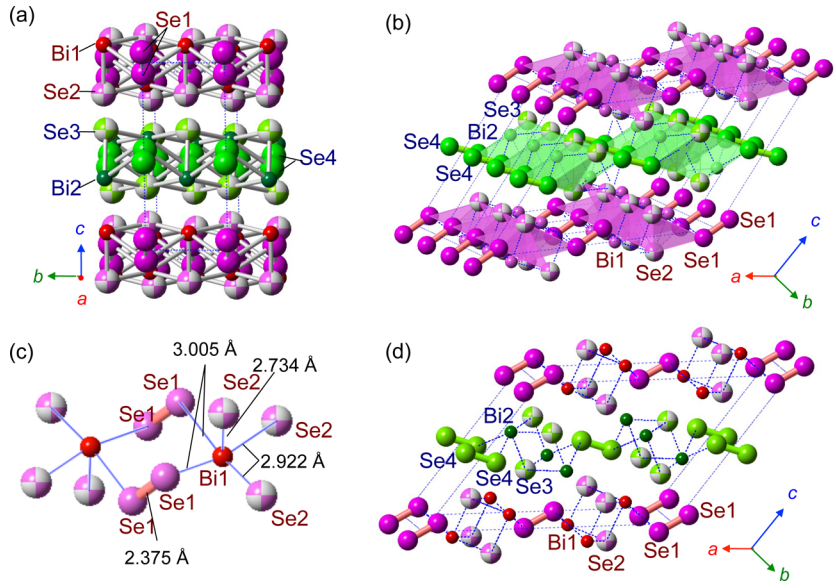

Figure 3. Crystal structure models of $BiSe_2$. (a) Ball-and-stick model of the *b*−*c* plane. (b) Bi−Se polyhedron model of the *a*−*b* plane. (c) Ball-and-stick model focused on a local structure with the Bi−Se bond distances. (d) Ball-and-stick model of the *a*−*b* plane. The small red and green balls are Bi1 and Bi2, the magenta and light-green balls Se1 and Se4, and large magenta and light-green balls with a checkered pattern Se2 and Se3, respectively.

pair of Bi may be positioned between layers, as anticipated from the local coordination.

The structures of BiSSe and BiS_2 were also refined using single crystals. They are isostructural with $BiSe_2$. The atomic positions are listed in parts b and c of Table 2, and the details of the refinement described in Supporting Information 1. Lattice parameters decrease with increasing sulfur content as naturally expected (Figure 1b and Table 1). The S1−S1 bond distance of 2.082 Å in is comparable to that of the reported S−S dimer such as pyrite-type FeS_2 (2.13 Å).[9] The bond-valence sum of Bi(+2.8, +2.9) in BiS_2 again ensures that Bi is nominally trivalent. Incidentally, the distribution between S and Se in BiSSe is not random. Selenium prefers to be positioned at the dimer, and sulfur is rather located at the single-ion position, as listed in Table 2b.

Here we compare the local structure of BiS_2 with that of the BiS_2 layer in the $LaO_{0.5}F_{0.5}BiS_2$ superconductor.[20] In both compounds, bismuth has five-fold coordination with sulfur

DOI: 10.1021/acs.inorgchem.5b00349
Inorg. Chem. 2015, 54, 4114−4119

pyramids, and the bond distances are very close to each other (2.597 and 2.534 Å for apical 2.827−2.847 and 2.873 Å for plane, respectively). The most distinct point is that the BiS_2 in $LaO_{0.5}F_{0.5}BiS_2$ is spread two-dimensionally, whereas a BiS_2 chain with a facing double BiS_5 pyramid is separated from the next BiS_2 chain by the S dimers. In the case of $LaO_{0.5}F_{0.5}BiS_2$, alternative stacking between the positive layer $[LaO]^+$ and the negative layer $[BiS_2]^-$ appears to stabilize the BiS_2 plane, into which carrier doping by F substitution [LaO] block is possible and leads to superconductivity. It would thus be interesting if carriers could be properly introduced into the quasi-one-dimensional BiS_2.

3.3. Chemical and Physical Properties of $BiSe_2$ and the Substitutions. To study the thermal stability of the high-pressure phases, we measured the weight change of $BiSe_2$, BiSSe, and BiS_2. When samples were heated with an Ar flow, the weight losses appear at 230−300 °C, as shown in Figure 4.

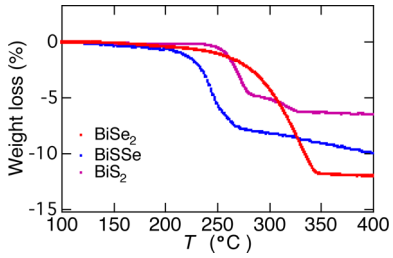

Figure 4. Thermal gravimetric analysis of $Bi(Se_{1-y}S_y)_2$ (y = 0, 0.5, or 1.0). The weight losses correspond to the transformation from $Bi(Se_{1-y}S_y)_2$ to $^1/_2Bi_2(Se_{1-y}S_y)_3$ and $^1/_2(Se_{1-y}S_y)$ (desorption).

We have examined the XRD patterns of samples quenched from the temperature regions with a weight plateau and inferred the following reaction.

$$BiX_2\ (X = Se\ or\ S) \rightarrow 1/2Bi_2X_3 + 1/2X\uparrow$$

The expected weight losses for $BiSe_2$, BiSSe, and BiS_2 were 10.7, 8.97, and 5.85%, respectively, and the actual losses were 12.0, 9.9, and 6.3%, respectively, being consistent with the process postulated above. The reason why the analyzed value is slightly larger than the expected one may be the fact that the excess selenium and/or sulfur could not be removed thoroughly and evaporated together with the main reaction. The decomposition temperature of $BiSe_2$ (285 °C) is higher than that of BiS_2 (256 °C). This step may result in breaking of the Se−Se and S−S bonds of the chalcogen dimers, and the Se−Se bond seems to be stronger than the S−S bond, probably because of higher covalency. The lower decomposition temperature for BiSeS (239 °C) may be attributed to the unstable bond between Se and S.

Magnetic and transport properties of the $BiSe_2$ and substitutions are shown in Figure 5. All the samples show diamagnetism with no temperature dependence (the small upturn below 20 K is perhaps due to a trace of magnetic impurities or trapped carriers), as shown in Figure 5a. This is attributed to the diamagnetic ion core with a closed shell. The absolute value agrees with the estimation from the sum of each ion,[21] which excludes the possibility of a Bi^{4+} state. As shown in Figure 5b, the electrical resistivity of these compounds is above 10^4 Ω cm below room temperature and shows a semiconducting behavior; the conductivity obeys the thermal activation rule, as shown in Figure 5c. The energy gap as estimated by the Arrhenius plot ranges from 0.28 to 0.69 eV,

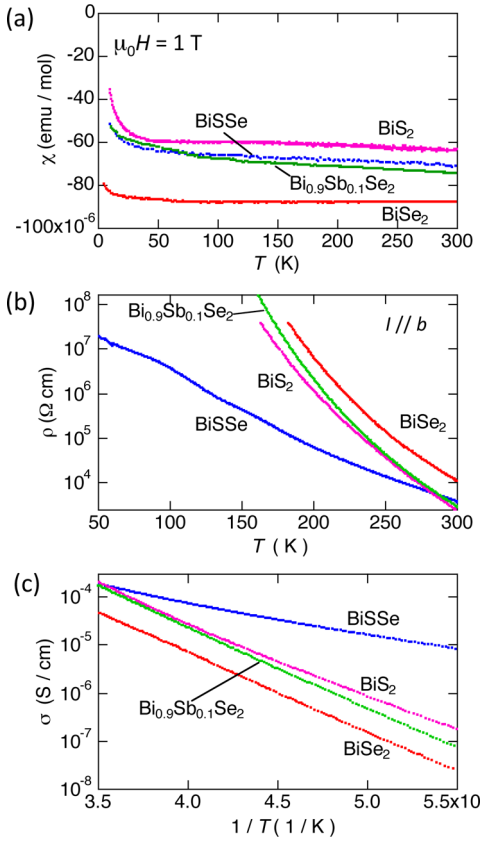

Figure 5. Physical properties of $BiSe_2$ and its substitutions. (a) Temperature dependence of dc susceptibility. (b) Temperature dependence of electrical resistivity. (c) Conductivity as a function of $1/T$.

being comparable to the band gaps of Bi_2Se_3.[22] Because the bandwidth of selenium is wider than that of sulfur, it was expected that the gap of $BiSe_2$ would be smaller than that of BiS_2. However, the values are almost the same in both $BiSe_2$ and BiS_2, while the activation energy in the mixed chalcogenide BiSSe is considerably smaller. The reason for the smaller activation energy is not clear; however, defects may produce extra carriers. It was also expected that a chemical pressure effect would reduce the resistivity in the Sb-substituted sample. However, there was no clear effect on the resistivity even though the lattice parameter becomes smaller.

To examine the topological character of the bismuth dichalcogenides, we have calculated the band structure of $BiSe_2$, as a representative compound of this group using the obtained crystal structure parameters and compared it against that of Bi_2Se_3, which is a well-known topological insulator. As shown in Figure 6, in $BiSe_2$, the conduction (valence) bands are predominantly made of the Bi 6p (Se 4p) orbitals for all k-points. The situation is nevertheless the same in Bi_2Se_3 except for the topmost valence band and bottommost conduction bands for which the respective orbital characters are interchanged at and in the vicinity of the Γ point. Such a band inversion is a characteristic feature for all topological insulators, including Bi_2Se_3. $BiSe_2$ does not show any band inversion around its band gap; therefore, it is a normal insulator. The calculated band gap for $BiSe_2$ is approximately 0.46 eV, which is within the range estimated from the temperature dependence of resistivity.

DOI: 10.1021/acs.inorgchem.5b00349
Inorg. Chem. 2015, 54, 4114−4119

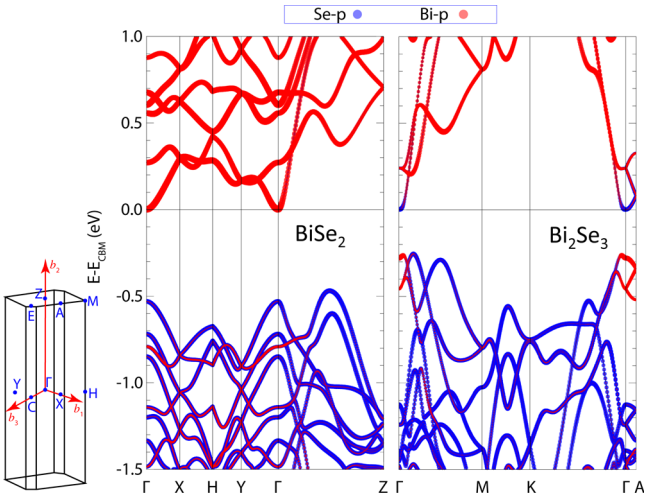

Figure 6. Electric band structure of $BiSe_2$ (left) and Bi_2Se_3 (right). The blue and red lines show Se 4p and Bi 6p character, respectively. The energy on the perpendicular axis was scaled with E_{CBM} (the energy of the conduction band minimum). In the case of Bi_2Se_3, the orbital characters of the topmost valence and bottommost conduction bands are interchanged at and in the vicinity of the Γ point, indicating a topological band inversion in this system. The corresponding Brillouin zone for $BiSe_2$ (Bi_2Se_3) is shown in the left side of the band structure.

Furthermore, we have tried to intercalate iodine into the pseudolayered compounds with the expectation of introducing a carrier and causing metallic charge transport, considering the case of Cu-intercalated Bi_2Se_3 showing superconductivity.[23] Reaction between iodine vapor and BiS_2 was conducted at relatively low temperatures (100−200 °C), but BiS_2 was attacked and decomposed into BiI_3 and other species. Further investigation is needed to determine the possibility of metallization in these compounds, including intercalation and partial substitution by other elements or molecules.

4. CONCLUSION

Single crystals of bismuth dichalcogenides $BiSe_2$ and BiS_2 have been successfully obtained by sintering at 5.5 GPa. The X-ray analyses show that $BiSe_2$, BiSSe, and BiS_2 have the same structure with a monoclinic cell. The unique characteristic of these compounds is the coexistence of single and dimerized chalcogen (X) ions in forms of X^{2-} and $(X_2)^{2-}$, while Bi is trivalent. They were diamagnetic semiconductors, and the nature of the topological insulator has not been determined.

■ ASSOCIATED CONTENT

Ⓢ Supporting Information

Crystallographic files in CIF format for $BiSe_2$, BiSSe, and BiS_2. This material is available free of charge via the Internet at http://pubs.acs.org.

■ AUTHOR INFORMATION

Corresponding Author

*E-mail: ayako-yamamoto@riken.jp.

Notes

The authors declare no competing financial interest.

■ ACKNOWLEDGMENTS

We thank Dr. Y. Tokunaga for helping with the resistivity measurement and Dr. H. Sakai, Mr. K. Saito, and Dr. S. Ishiwata for preliminary experiments on Cu intercalation. This work was supported by the Cabinet Office, Government of Japan, and the Japan Society for the Promotion of Science (JSPS) through the Funding Program for World-Leading Innovative R&D on Science and Technology (FIRST Program). M.S.B. was partly supported by a grant-in-Aid for Scientific Research (S) (No. 24224009) from the Ministry of Education, Culture, Sports, Science and Technology (MEXT) of Japan.

■ REFERENCES

(1) Scherrer, H.; Scherrer, S. In *Handbook of Thermoelectrics*; Rowe, D. M., Ed.; CRC Press: New York, 1994; pp 211−237.
(2) Ando, Y. *J. Phys. Soc. Jpn.* **2013**, *82*, 102001.
(3) Atabaeva, E. Ya.; Bendeliani, N. A.; Popova, S. V. *Fiz. Tverd. Tela* **1973**, *15*, 3508−3512.
(4) Vereshagin, L. F.; Atabaeva, E. Ya.; Bendeliani, N. A. *Fiz. Tverd. Tela* **1971**, *13*, 2452−2454.
(5) Nakayama, A.; Einaga, M.; Tanabe, Y.; Nakano, S.; Ishikawa, F.; Yamada, Y. *High Pressure Res.* **2009**, *29*, 245−249.
(6) Silverman, M. S. *Inorg. Chem.* **1964**, *3*, 1041−1042.
(7) Silverman, M. S. *Inorg. Chem.* **1965**, *4*, 587−588.
(8) Jobic, S.; Deniard, P.; Brec, R.; Rouxel, J.; Drew, M. G. B.; David, W. I. F. *J. Solid State Chem.* **1990**, *89*, 315−327.
(9) Rummery, T. E.; Heyding, R. D. *Can. J. Chem.* **1966**, *45*, 131−137.
(10) Evans, H. T., Jr.; Konnert, J. A. *Am. Mineral.* **1976**, *61*, 996−1000.
(11) Mizuguchi, Y.; Demura, S.; Deguchi, K.; Takano, Y.; Fujihisa, H.; Gotoh, Y.; Izawa, H.; Miura, O. *J. Phys. Soc. Jpn.* **2012**, *81*, 114725.
(12) Usui, H.; Suzuki, K.; Kuroki, K. *Phys. Rev. B* **2012**, *86*, 220501R.
(13) Blaha, P.; Schwarz, K.; Madsen, G.; Kvasnicka, D.; Luitz, J. *WIEN2K* (http://www.wien2k.at).
(14) Vicente, C. P.; Tirado, J. L.; Adouby, K.; Jumas, J. C.; Toure, A. A.; Kra, G. *Inorg. Chem.* **1999**, *38*, 2131−2135.
(15) Bremholm, M.; Hor, Y. S.; Cava, R. J. *Solid State Sci.* **2011**, *13*, 38−41.
(16) Gronvold, R.; Rost, E. *Acta Crystallogr.* **1957**, *10*, 329−331.
(17) Shannon, R. D.; Prewitt, C. T. *Acta Crystallogr.* **1969**, *B25*, 925−945.
(18) Gardes, B.; Brun, G.; Tedenac, J. C. *Eur. J. Solid State Inorg. Chem.* **1989**, *26*, 221−225.
(19) Bronsema, K. D.; de Boer, J. L.; Jellinek, F. *Z. Anorg. Allg. Chem.* **1986**, *540*, 15−17.
(20) Miura, A.; Nagao, M.; Takei, T.; Watauchi, S.; Tanaka, I.; Kumada, N. *J. Solid State Chem.* **2014**, *212*, 213−217.
(21) Selwood, P. W. *Magnetochemistry*, 2nd ed.; Interscience Publishers Inc.: New York, 1956. Morrish, A. H. *The Physical Principles of Magnetism*; John Wiley & Sons, Inc.: New York, 1965.
(22) Xia, Y.; Qian, D.; Hsieh, D.; Wray, L.; Pal, A.; Lin, H.; Bansil, A.; Grauer, D.; Hor, Y. S.; Cava, R. J.; Hasan, M. Z. *Nat. Phys.* **2009**, *5*, 398−402.
(23) Kriener, M.; Segawa, K.; Ren, Z.; Sasaki, S.; Ando, Y. *Phys. Rev. Lett.* **2011**, *106*, 127004.

DOI: 10.1021/acs.inorgchem.5b00349
Inorg. Chem. 2015, 54, 4114−4119